STUDY OF THE CRACK GROWTH IN COMPOSITE ROTOR BLADE SKIN

T. Rouault[1,2*], V. Nègre[2], C. Bouvet[1], P. Rauch[2]
[1] Université de Toulouse ; ISAE, INSA, UPS, EMAC ; ICA (Institut Clément Ader) ; ISAE, 10 av. E. Belin, 31055 Toulouse, France
[2] Eurocopter, 13725 Marignane, France
vincent.negre@eurocopter.com

Abstract

The phenomenon of through-the-thickness crack growth in rotor-blade skin was studied in this paper. Experimental investigations were carried out to characterize damage phenomena with quasi-static and fatigue test on coupons made of blade skin materials. Observations lead to an original modeling approach to simulate fatigue crack growth, which was implemented into FE software. Experimental tests and numerical simulations of crack growth under fatigue loading on samples representative of in-flight load were conducted to evaluate the accuracy of the modeling. Crack path, crack propagation speed, and damage area measured and simulated were compared.

1. INTRODUCTION

In rotorcrafts, blades are among the most critical components. They undergo a high cycle fatigue of a complex multi-axial loading and a close attention has to be paid to the safety of their design. We can roughly consider the structure of a blade as a stiff spar and a foam filling covered with a thin composite material skin. In case of foreign object impact or unexpected stress concentration, a through-the-thickness crack, (also called “translaminar crack” [1]) can initiate on the skin. For a fail-safe design of blades, this damage phenomenon has to be understood and its potential propagation along the skin has to be quantified. For that purpose, crack propagation experiments on rotor blades have been carried out in Eurocopter. Besides, a study is currently conducted with Institut Clément Ader, (Toulouse) for several years in order to understand the phenomenon and to develop a numerical modelling to simulate crack propagation [2][3][4]. The study focuses on glass fibre based, woven composite materials with $[0/90]_n$ and $[+-45]_n$ stacking sequences where *n* is small (2 or 4). First, experiments were carried out on small samples to study the effect of static and fatigue loadings on the material. Samples were cut out and polished to observe the damaged material with the aid of optical microscopy and scanning electron microscopy (SEM). It revealed that the type of damage was different for tension and shear loadings. Then, propagation tests were carried out on structural shaped samples under cyclic tension-tension and shear loading, to simulate opening and in-plane shear failure mode on blade skin (figure 1)

It was shown that in fatigue loading, when a through-the-thickness crack propagates, a fibre bundle can only collapse entirely [2]. Thus, the crack propagation speed is strongly dependant on the width of the fibre bundle and an original propagation modelling has been developed according to this observation. Between the micro-scale approach aiming at representing separately the two components of the material, and macro-scale models where properties are homogenized and continuum damage mechanics is used, we developed a modelling where the material is meshed according to the bundle width, in order to understand the behaviour of a notched woven composite and predict the propagation of the crack under cyclic loading.

More accurately, in this approach, two oriented meshes representing the warp and weft directions of the woven fabric are superimposed. Each tow is represented by one row of quadrangles, and spring elements link warp and weft tows to each other (see figure 5). These interface elements contain all the potential damages of the material through their evolving stiffness. The stiffness of spring elements can evolve as a function of static and fatigue loading. Finally, we consider with respect to experimental observations that a bundle can only break entirely and failure interface elements are introduced so that each bundle can break. We use a fatigue curve, and a cumulative Miner-Palmgren's law to compute the damage into each tow and determine which one is critical and how many cycles it can sustain before its failure. It is then possible to deduce the direction of the propagation, its speed, and the extent of damage area. Besides, for the particular application of this study, considering the high stiffness of the spar, displacement field is supposed constant sufficiently far from the crack. Structural tests are then represented by experimental and numerical strain controlled tests, and the fatigue law we use is an ε-N curve.

2. STUDY OF THE DAMAGE

The material studied is an 8-harness satin weave glass-epoxy composite. Quasi-static stress-strain responses under tension and shear loading for a $[0/90]_2$ are shown in Figure 2.

An investigation was carried out to characterize damage form for this particular material under cyclic loadings. Several studies describe micro-cracks in transverse yarns under quasi-static tension on woven laminates [5] [6]. To compare with static damage form, cyclic tension-tension loadings were applied to samples and fragments were cut out and polished to observe the damaged material with the aid of SEM. Figure 3 shows some results of SEM visualisation of a damaged sample through different sections. Damage is found to be similar as in quasi-static, without noticeable crack density increase as there is no more than one or two micro-cracks in each bundle.

The same work was carried out on shear samples. A rail-shear test experiment in accordance with D4255 ASTM norm [7] was used to study the damage on samples under cyclic shear loading. Though we observe a decrease of about 15% of the shear modulus, and we increased the load to high strain (higher than 3%), no SEM observation has revealed any crack (Figure 4) contrary to the tension case. Stress intensity factors involving micro-cracks might be much lower in shear than in tension. Moreover, it seems that epoxy resin strength is much higher in shear than in tension, as already noticed for this type of matrix which strength is said to be sensitive to the hydrostatic part of the stress tensor [8]. The macroscopic loss of stiffness and inelastic strains are consequently attributed to lower scale polymer damage.

3. MODELLING APPROACH

Since tow width seems to be a relevant parameter for propagation phenomenon, the FE mesh has been adapted to this dimension. Then, each tow is meshed with a raw of quadrangles. As a crack propagates under cyclic loading, it has been noticed that a tow can only break entirely [2]. Failure elements have been introduced between each quadrangle so that failure can happen between each element (Figure 5). Their failures involve the fracture of the tow in its whole width in accordance with experimental observations.

The two reinforcement directions are meshed with this technique and the two resulting meshes are superimposed, so that warp and weft nodes share identical coordinates. They are linked each others with two nodes interface elements represented by springs (Figure 6) as some authors already employed for delamination modelling [9] [10] [11]. These elements link stiffly the two reinforcement directions. The softening law of these springs aims at simulating damage in the interface.

This resulting damage is then localized in interface elements and not homogenised as usually represented in continuum damage mechanics with continuous damage variables [12]. However, a relationship between uniform damage and spring interface elements stiffness can be formulated. Constitutive law of spring elements can then be identified with experimental measure of longitudinal modulus decrease.

The tow weaving is not represented in this modelling. It corresponds to a micro-scale approach (e.g. [13] [14]), in which numerous additional parameters (3D-shape of bundles, strain field in bundles resulting of macro-loading, damage law as a function of the relative position to crossover points) are taken into account. This approach has not been found appropriate for the present application which aims at modelling phenomenon on a complete structure with a small number of material and architectural parameters.

3.1. Degradation under tension

Under tension-tension fatigue loading, damage appears through a loss of longitudinal stiffness. Damage is introduced through stiffness decrease in spring interface elements. The initial stiffness is initially numerically infinite (sufficiently high value), and it decreases as a function of the sustained strain, and the number of cycles. In the actual modelling, interface elements collect longitudinal strain in neighbouring quadrangle elements. This modelling thereby uses a kind of communication between elements of different types.

The evolution of longitudinal damage, *d*, has been determined by experimental tension-tension fatigue tests on $[0/90]_2$ laminate samples. The young modulus *E* has been measured at regular intervals and compared to initial young modulus E_0. *d* is defined by:

(1) $$d = 1 - \frac{E}{E_0}$$

A damage evolution law can be derived from experimental fatigue results:

(2) $$\frac{\partial d}{\partial N} = f(d, \varepsilon_{max}, R)$$

where *N* is the number of cycles, ε_{max} is maximum strain achieved during a fatigue cycle and $R = \varepsilon_{min} / \varepsilon_{max}$ is the load ratio. To limit the number of test, this last parameter has been set to a value of 1/3 for every fatigue and propagation experiments. This value has been chosen to be appropriate to reproduce the variable in-flight loading on blade skin with only one load ratio.

3.2. Degradation under shear

As showed in the previous part, under shear loading, damage is not produced by some micro-cracks, but it appears diffusely. Moreover, anelastic strains appear due to matrix pseudo-plasticity. These ones appear for much higher strains than in-flight strains, but around the notch tip, such high strain can be achieved. According to the diffuse aspect of this phenomenon, the shear behaviour and pseudo-hardening has been implemented into the constitutive law of 2D-elements. Viscosity shown in shear test results is not taken into account. The simulated shear behaviour is compared to experimental one on Figure 7.

3.3. Fibre degradation

Single fibres are generally assumed linear elastic non-damageable. As the test proceeds and the crack progresses, the strain field is modified. Every single bundle sustains a cyclic loading with evolving amplitude. To predict its failure, a cumulative fatigue damage law is needed. The most commonly used one on metallic or composite materials is Miner-Palmgren's law, because of its simplicity [15]:

$$D = \sum \frac{n_i}{N_i} \quad (3)$$

where n_i is the number of cycles sustained at level i and N_i number of cycle to failure for a fatigue loading at constant amplitude i. Failure happens when the value of Miner's fraction of life D reaches 1. This law is implemented in the modelling and Miner's damage fractions of life are attributed to each failure interface elements. It is well known that this law is not really efficient for composite materials especially because the sequence effect is not taken into account [16], but its simplicity and the lack of relatively basic law consistent with a wide range of composite materials makes it still the most widely used.

$N_i(\varepsilon_i)$ law (ε-N curve), was derived from fatigue experiments data. It is noteworthy to point out that the strategy to compute crack growth speed does not use classical fracture mechanics and energy release rate, but a lifetime curve ε-N to estimate the number of cycles to failure for each bundle. Significant damage observed at the crack tip, especially matrix micro-cracks into bundles inhibit load transfer between bundles and thus relax stress concentration. In the modelling, interface elements degradation leads to a sliding between bundles and makes the crack tip not sharp. It prevents stress singularity in bundle elements and allows the use of a fatigue law for fibre failure.

3.4. Fibre failure

Failure happens tow by tow consistently with experimental observations by failure interface elements. These elements have binary behaviour. Failure happens when damage fraction of life of one neighbouring element reaches 1.

3.5. Simulation management

The modelling has been implemented on commercial finite element code SAMCEF and run with implicit method. A simulation is divided into sequences. A sequence corresponds to a loading with settlement of damage, and failure of one element (progression of the crack by the length of one element). At the maximum strain of each sequence, the number of cycles to failure of the next bundle (the one which Miner's fraction of life D will reach 1 the sooner) is computed. At failure of the bundle, the number of cycles to failure is added to the total number of cycles, and damage of other elements is updated.

4. RESULTS

The modelling was applied to simulate tension-tension fatigue tests on structural samples on $[\pm 45]_2$ laminates. The experimental methodology of the test and design of the structural samples are detailed in [3]. It was also compared with results of notched rail shear test experiments on $[0/90]_4$ laminates.

4.1. $[\pm 45]_2$ tension results

The Figure 8 shows the warp and weft meshes corresponding to +45° and -45° tows after propagation. The simulated averaged direction of propagation appears to be orthogonal to the tension direction, where mode I energy release rate is maximum. Thus, the crack propagation breaks up alternatively a warp and a weft tow as noticed on experimental tests.

The numerical damage area can also be evaluated, in plotting the spring interface elements stiffness field (Figure 8 – bottom-right) which points out damage area. It can be compared with the experimental picture (top right) where resin whitening is noticed. It reveals damage matrix area (darker on the picture) of a few millimetres width, at each side of the crack, and dark micro-cracks lines in ±45° directions, parallel to bundles.

Crack propagation speed as a function of crack length has been computed and compared to experimental one in Figure 9. A good correlation is found as the speed decreases with the development of the crack. However, strong variations are superimposed to the main tendency of the curve. They can be attributed to the severe degradation of interface elements stiffness around failure. Some other phenomena such as threshold effect can also be related to this shape of the curve.

4.2. $[0/90]_4$ shear results

The three rails shear test used for shear experiments was employed to carry out crack propagation experiments under shear fatigue loading. A pre-crack was introduced on one side of the sample (See scheme on Figure 10b). The crack first spread downward and then it inflects toward one side to become nearly orthogonal to the tensile principal strain (Figure 10c). Darker areas shaped like small droplets develop under the crack.

The pixel-to-pixel difference between images at different times was computed. It can reveal damage area evolution between two instants. The difference between initial image and the crack after 7 millions of cycle is shown Figure 10e. Brighter pixels correspond to greater difference and consequently colour evolution. One can observe that the damage area spread almost 20mm below the crack tip.

Numerical results show a crack direction almost inclined to 45 degrees to the initial notch (Figure 10a). As for $[\pm 45]_2$ tension tests, warp tows breaks alternatively with weft tows, in quite good accordance to experimental test since crossover points of the ply are not taken into account.

Stiffness field of spring interface elements has been plotted and reported in Figure 10d. The most severe degradations are concentrated along the crack. Below the crack, a slight damage area is noticeable. Its shape can be compared to experimental post processed image which correspond to a map of the resin whitening.

Experimental and simulated crack propagation speeds were compared on Figure 11. In spite of uncertainty on method to extract crack length from pictures, a good agreement is found. The modelling reproduces fairly the decrease of crack propagation speed and the average value of the speed.

4.3. Discussion

Basically results obtained with this methodology concerning the extent of damaged area and crack propagation speed, are promising even without considering crossover points. We can mention that initiation of the crack is not well-rendered. This initiation time is strongly dependant on numerous parameters among which local microstructure aspects (position and aspect of the crack tip relatively to bundles, crossover points, position of plies relatively to each other's…) which reasonably can't be controlled. It can explain the considerable scatter in initiation number of cycles noticed [2] and the difficulty to predict it numerically.

Besides, it's more of interest to estimate propagation speed. An incident, such as foreign object impact on the blade skin can lead to fibre failures and trigger a through-the-thickness crack [17]. Criticality of this damage for the blade can be evaluated by the kind of modelling presented above. The propagation mesh (tow by tow) can be integrated into an existing complete blade mesh. By the use of numerical tools such as super-elements, in-flight loading conditions can be transposed on the contour of the propagation mesh. This kind of simulation and its comparison to crack propagation experiments on rotor blades will be performed.

5. Conclusion

A phenomenological approach has been carried out to simulate the propagation of a through-the-thickness crack on rotor blade skin under in-flight fatigue loading. The damage phenomenon were analysed and represented into a modelling which combines semi-discrete damage and cumulative fatigue law. Simulations have been compared to numerous experimental results on tension-tension and shear fatigue tests on coupons. The representation of the phenomenon is now well mastered and the propagation mesh is mature enough to be adapted to the modelling of a full blade. We are one step away from having a tool able to simulate crack propagation on a complete blade structure.

References

[1] M. J. Laffan, S. T. Pinho, P. Robinson, et A. J. McMillan, « Translaminar fracture toughness testing of composites: A review », *Polymer Testing*, 2012.

[2] M. Bizeul, C. Bouvet, J. J. Barrau, et R. Cuenca, « Influence of woven ply degradation on fatigue crack growth in thin notched composites under tensile loading », *International Journal of Fatigue*, vol. 32, n°. 1, p. 60–65, janv. 2010.

[3] M. Bizeul, C. Bouvet, J. J. Barrau, et R. Cuenca, « Fatigue crack growth in thin notched woven glass composites under tensile loading. Part I: Experimental », *Composites Science and Technology*, vol. 71, n°. 3, p. 289–296, févr. 2011.

[4] T. Rouault, C. Bouvet, M. Bizeul, et V. Nègre, « Modélisation de la propagation d'une coupure sur stratifié mince de composite tissé soumis à un chargement cyclique de traction », presented at the 17èmes Journées Nationales sur les Composites (JNC17),, Poitiers-Futuroscope□: France, 2011.

[5] F. Gao, L. Boniface, S. L. Ogin, P. A. Smith, et R. P. Greaves, « Damage accumulation in woven-fabric CFRP laminates under tensile loading: Part 1. Observations of damage accumulation », *Composites Science and Technology*, vol. 59, n°. 1, p. 123–136, janv. 1999.

[6] T. Osada, A. Nakai, et H. Hamada, « Initial fracture behavior of satin woven fabric composites », *Composite Structures*, vol. 61, n°. 4, p. 333–339, sept. 2003.

[7] « ASTM D4255/D4255M-83: Standard Guide for Testing In-Plane Shear Properties of Composite Laminates (Two- and Three-Rail Shear Test) ». 1994.

[8] B. Fiedler, M. Hojo, S. Ochiai, K. Schulte, et M. Ando, « Failure behavior of an epoxy matrix under different kinds of static loading », *Composites Science and Technology*, vol. 61, n°. 11, p. 1615–1624, sept. 2001.

[9] J. C. J. Schellekens et R. De Borst, « Numerical simulation of free edge delamination in graphite-epoxy laminates under uniaxial tension », *Composite Structures*, p. 647–657, 1991.

[10] D. Xie et A. M. Waas, « Discrete cohesive zone model for mixed-mode fracture using finite element analysis », *Engineering Fracture Mechanics*, vol. 73, n°. 13, p. 1783–1796, sept. 2006.

[11] M. R. Wisnom et F.-K. Chang, « Modelling of splitting and delamination in notched cross-ply laminates », *Composites Science and Technology*, vol. 60, n°. 15, p. 2849–2856, nov. 2000.

[12] J.-L. Chaboche, « Continuous damage mechanics — A tool to describe phenomena before crack initiation », *Nuclear Engineering and Design*, vol. 64, n°. 2, p. 233–247, avr. 1981.

[13] A. R. Melro, P. P. Camanho, F. M. Andrade Pires, et S. T. Pinho, « Numerical simulation of the non-linear deformation of 5-harness satin weaves », *Computational Materials Science*, vol. 61, p. 116–126, août 2012.

[14] G. Couégnat, E. Martin, et J. Lamon, « 3D multiscale modeling of the mechanical behavior of woven composite materials »,

presented at the ICCM 2010, Budapest, 2010.
[15] J. A. Epaarachchi et P. D. Clausen, « A new cumulative fatigue damage model for glass fibre reinforced plastic composites under step/discrete loading », *Composites Part A: Applied Science and Manufacturing*, vol. 36, n°. 9, p. 1236–1245, sept. 2005.
[16] W. V. Paepegem et J. Degrieck, « Effects of Load Sequence and Block Loading on the Fatigue Response of Fiber-Reinforced Composites », *Mechanics of Advanced Materials and Structures*, vol. 9, n°. 1, p. 19–35, 2002.
[17] P. Navarro, J. Aubry, S. Marguet, J.-F. Ferrero, S. Lemaire, et P. Rauch, « Experimental and numerical study of oblique impact on woven composite sandwich structure: Influence of the firing axis orientation », *Composite Structures*, vol. 94, n°. 6, p. 1967–1972, mai 2012.

Figures

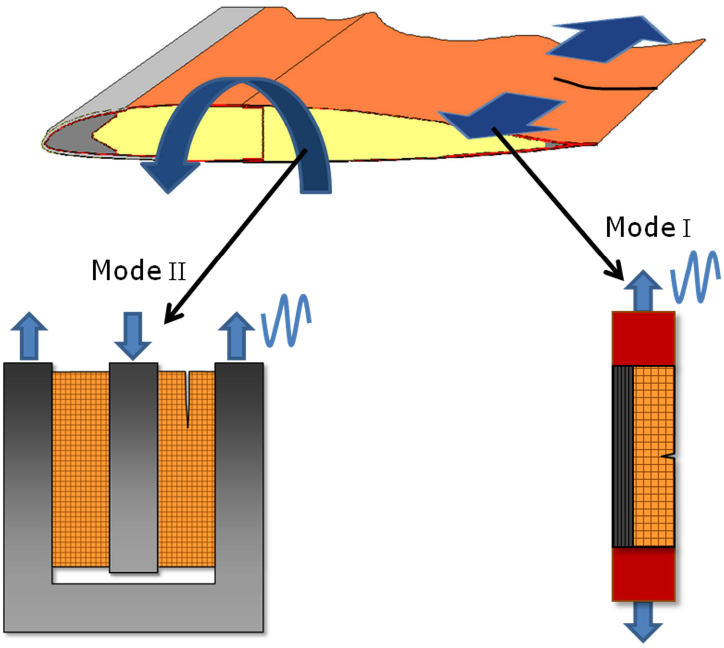

Figure 1 – Illustration of the experimental approach: a tension loading on a rotor-blade implies a mode I failure, simulated by a cyclic tension test on a structural sample. On the other hand, torsion loading involves mode II failure represented by a rail shear experiment.

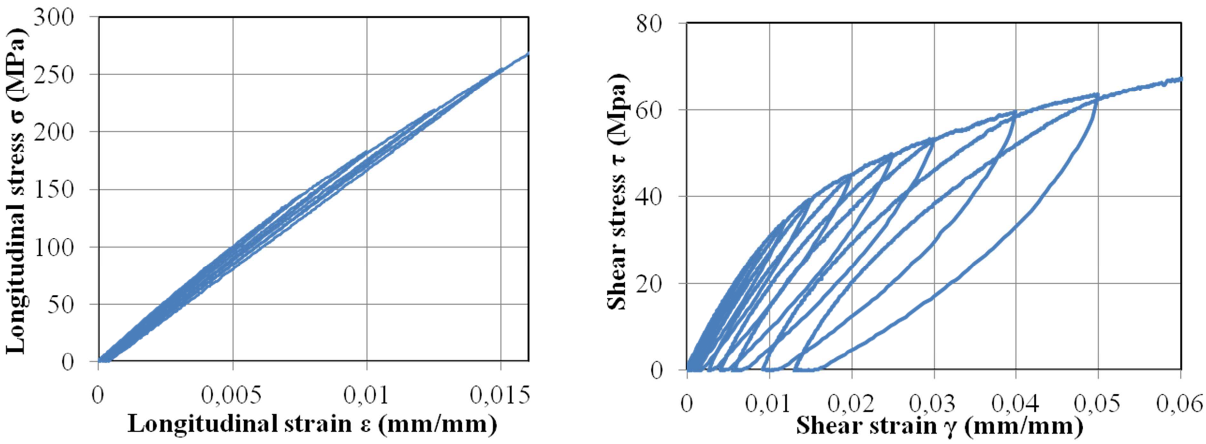

Figure 2 – Stress-strain response under tension (left) and shear (right) loading of a $[0/90]_4$ laminate of the studied material. Charge and discharge were applied to evaluate rigidity and inelastic strain evolution.

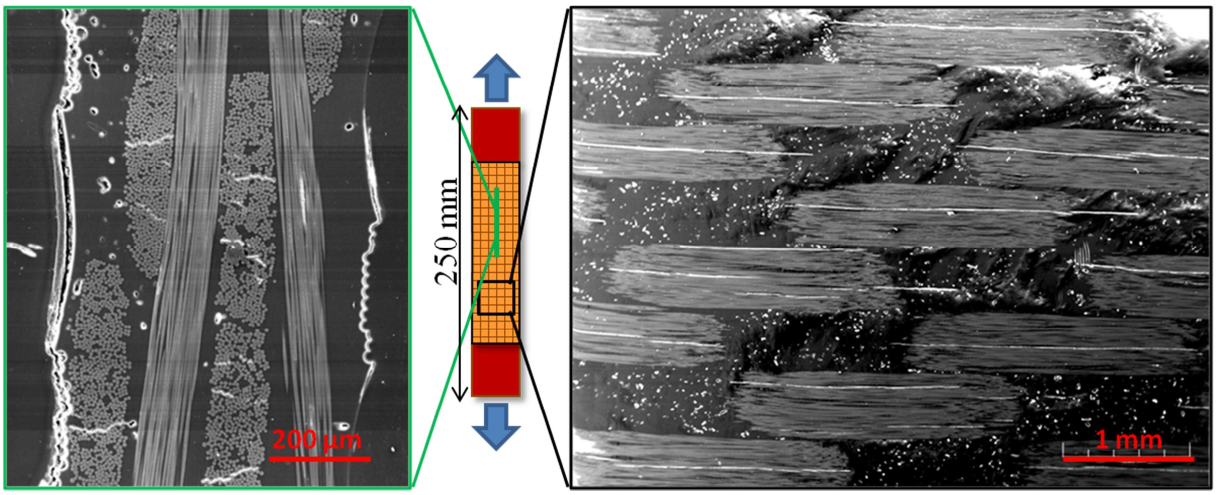

Figure 3 – Damage in a woven GFRP under tension-tension fatigue loading after 5.10^4 cycles at 1% maximum longitudinal strain.

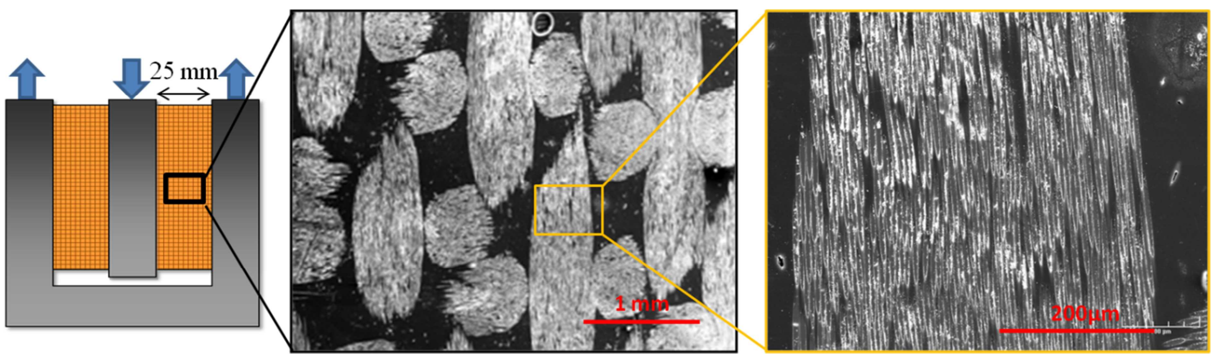

Figure 4 – SEM micrography of the surface of a sample after high strain cyclic loading.

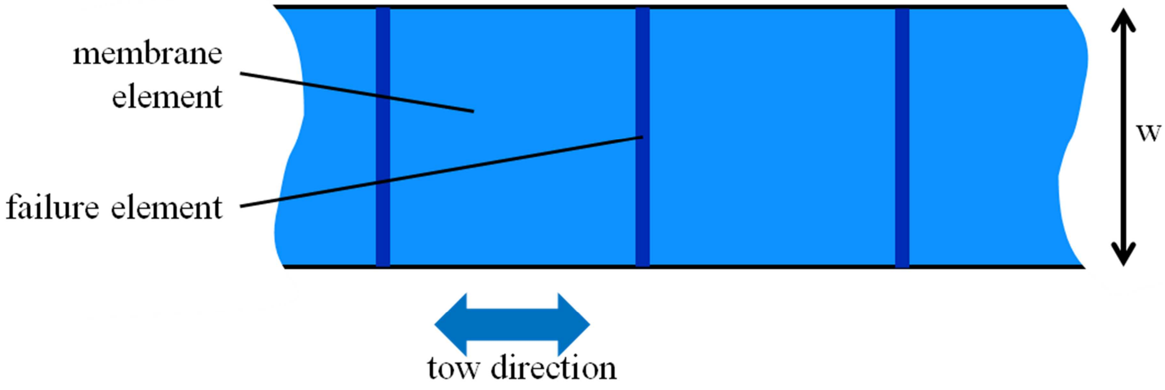

Figure 5 – Modelling of a single bundle meshed by a raw of quadrangles separated by failure interface elements.

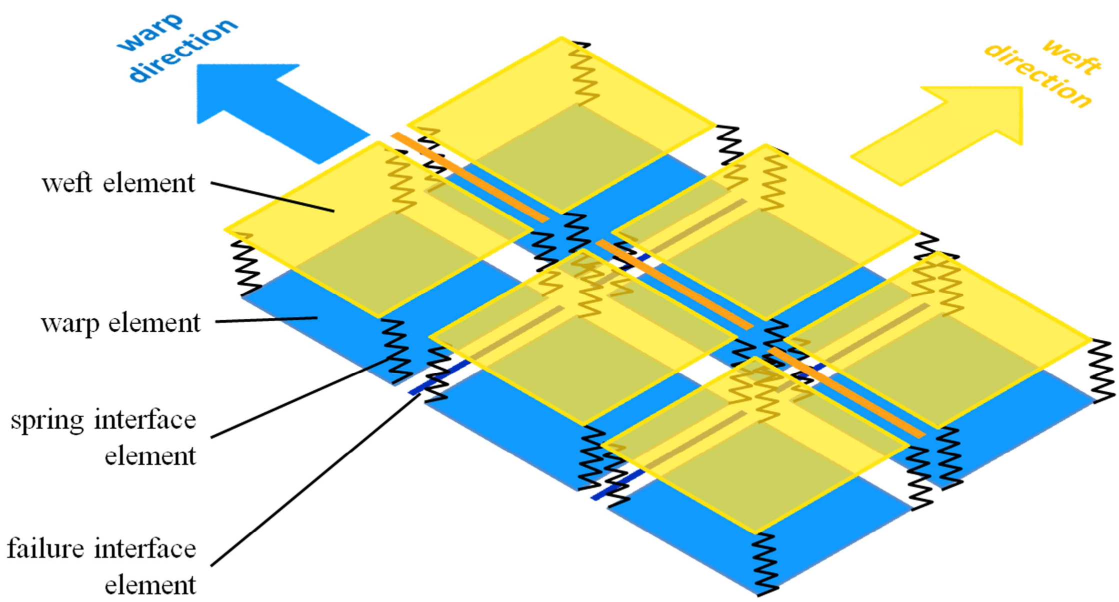

Figure 6 – Modelling principle. The two superimposed meshes are represented separately for more clarity. Consequently, spring interface elements and failure elements sizes, is non zero on the figure.

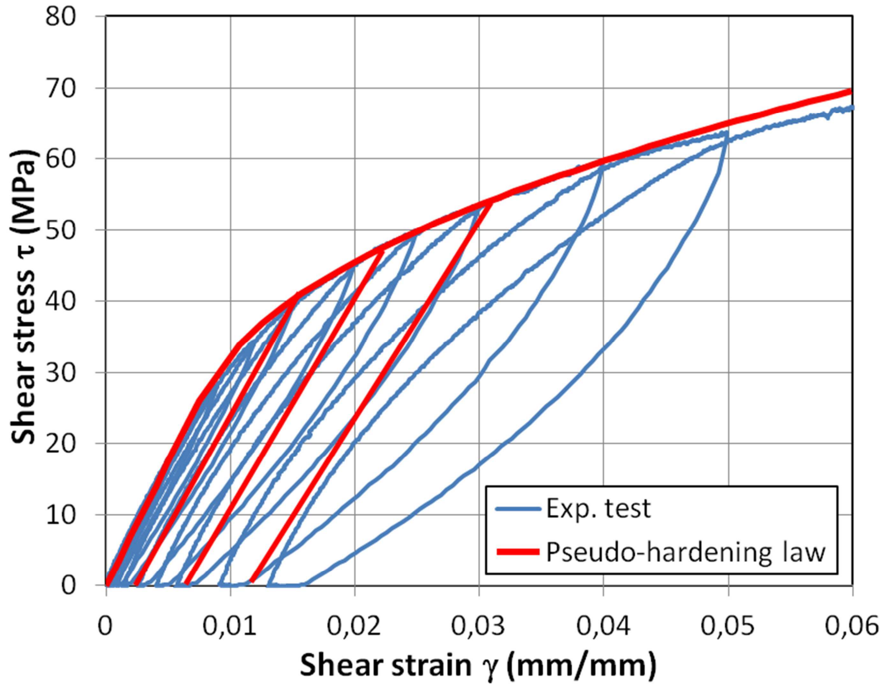

Figure 7 – Identification of the pseudo-hardening law in shear from experimental results

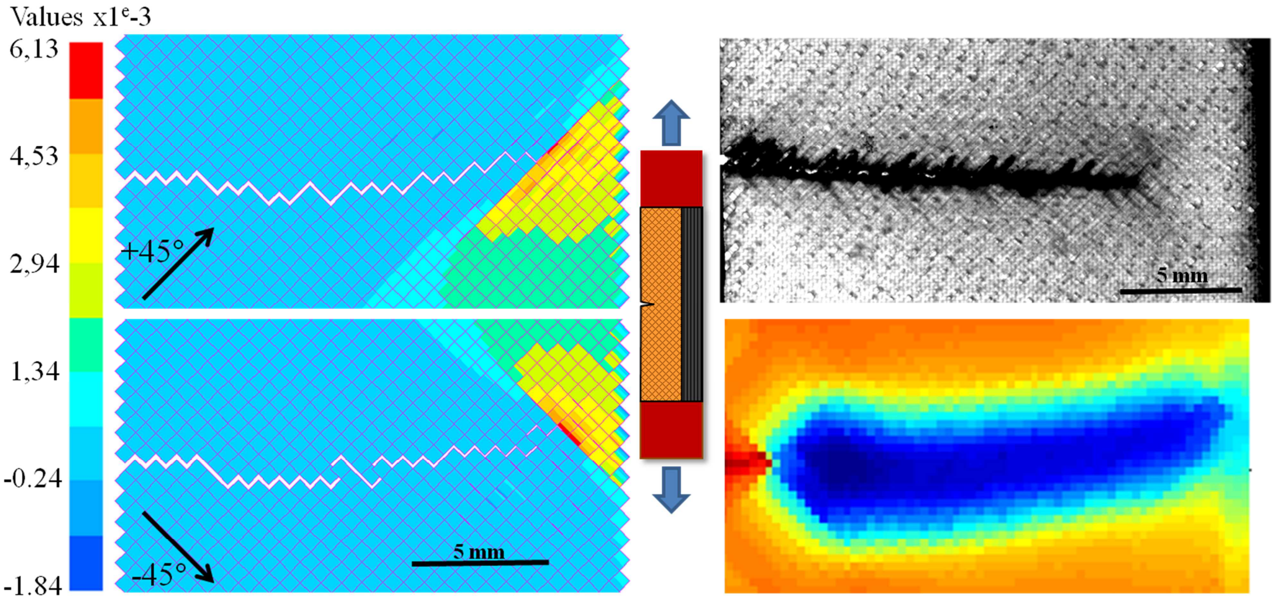

Figure 8 – Comparison between experiments and simulation on [±45]$_2$ fatigue tensile crack growth. Left: longitudinal strain in warp and weft bundles. Top-right: photography of the crack at the end of the test. Bottom-right: stiffness field of spring interface elements.

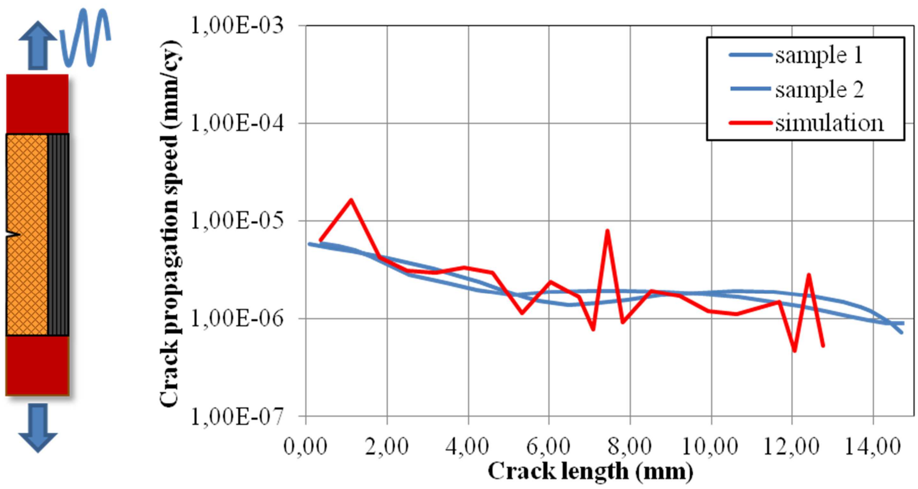

Figure 9 - Comparison between experimental and simulated crack propagation speeds.

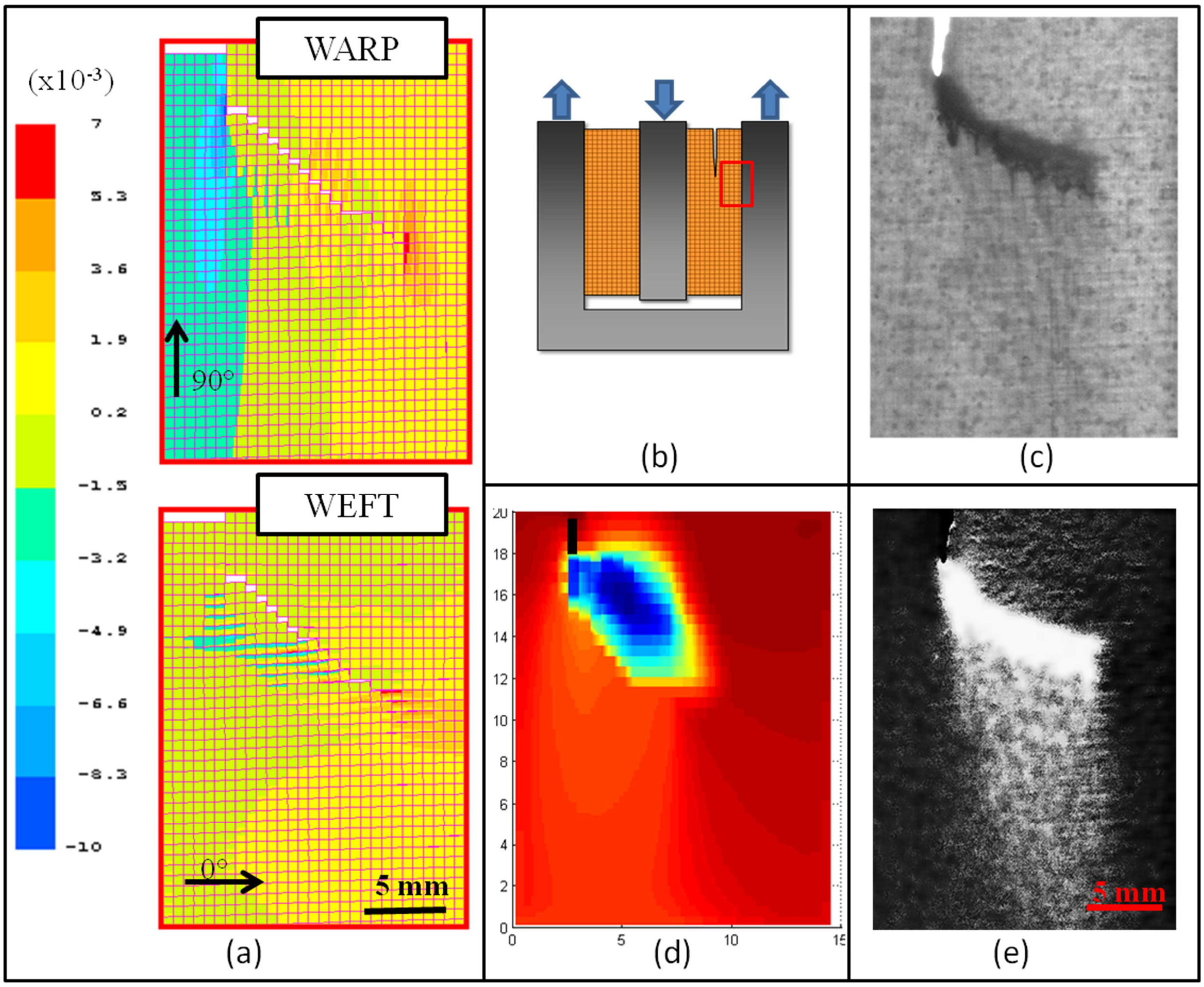

Figure 10 - Comparison between experiments and simulation on $[0/90]_4$ fatigue shear crack growth. (a): longitudinal strain in warp and weft bundles. (b): scheme of the experiment. (c): photography of the crack at the end of the test. (d): Stiffness field of spring interface elements. (e): post-processed picture revealing damaged zone in the experimental test.

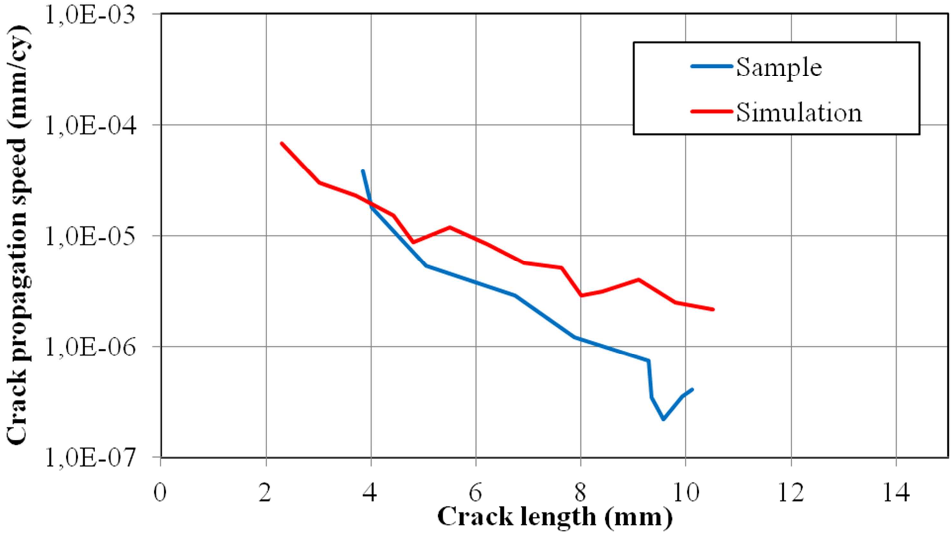

Figure 11 – Comparison between experimental and simulated crack propagation speed on $[0/90]_4$ shear fatigue test.